JOURNAL OF PROPULSION AND POWER
Vol. 12, No. 6, November–December 1996

Near-Electrode Model for 100-Standard Atmosphere Arc Discharges

E. J. Felderman,* W. N. MacDermott,† and C. J. Fisher‡
Arnold Engineering Development Center, Arnold Air Force Base, Tennessee 37389–9013

The near-electrode region is important to the design of high-pressure electric arc heaters. An understanding of the detailed physics of the discharge in the immediate region around the attachment to the electrode surfaces, where there is a rapid transition from gaseous to solid-state conduction of electrical current, is key to understanding such issues as electrode erosion and survival. A continuum model for the near-electrode region at high pressure is presented, extending from the flow region all the way into a copper electrode. The gaseous part of the model is treated with a one-dimensional approximation, and the heat conduction in the solid material is analyzed in a three-dimensional reference frame that moves with the arc attachment spot. Experimental data on the near-electrode region of high-pressure arc heaters are very limited, they mainly consist of dimensions of arc tracks and mass-loss measurements. Incorporating a field-emission boundary condition at the cathode spot and a nonequilibrium electron temperature at the anode spot yields results that agree with the data.

Nomenclature

A = area, cm^2
A_R = Richardson coefficient, A/(cm K)^2
B = dimensionless half-width, $Ub/2K$
B_i = induced magnetic field, T
b = half-width of square spot, m
CR = current contraction parameter, Eq. (2)
C_1 = constant, Eq. (12)
C_2 = constant, Eq. (12)
c = average molecular speed, m/s
d = diameter, mm
E = electric field, V/m
e = electron charge, C
I = current, A
J = current density, A/cm^2
K = thermal diffusivity, cm^2/s
k = thermal conductivity, W/cm K
k_B = Boltzmann constant, J/K
L_c = thickness of current concentration zone, cm
m = molecular mass, kg
$\dot{m}$ = mass rate, kg/s
n = number density, cm^{-3}
P = pressure, atm
Q = collision cross section
q = heat flux, MW/cm^2
r = radius, cm
T = temperature, K
t = time, s
U = arc spot velocity, m/s
u = dummy variable of integration, Eq. (9)
X = normalized coordinate, $Ux/2K$
x, y, z = Cartesian coordinates, origin on surface of electrode. z normal to surface, + outward for gas phase solution, + inward into copper for solid-state solution; x is + in direction of U; y is transverse to U, m
Y = normalized coordinate, $Uy/2K$
Z = normalized coordinate, $Uz/2K$
ΔT = temperature rise in copper, K
δ_h = nonelastic collision factor
ε_0 = permittivity of free space, 8.85×10^{-12} F/m
μ_0 = magnetic permeability of free space, $4\pi \times 10^{-7}$ H/m
σ = electrical conductivity, $(\Omega\ \text{cm})^{-1}$
ϕ = work function for copper, eV

Subscripts
AN = anode
a = arc
CA = cathode
Cu = copper
c = current concentration zone
cond = condensation
Eq = equilibrium
e = electron
evap = evaporation
f = flow affected region
g = heavy gas particle
s = spot
w = wall
0 = reference value

Received Nov. 2, 1994; revision received March 5, 1996; accepted for publication May 10, 1996. This paper is declared a work of the U.S. Government and is not subject to copyright protection in the United States.

*Senior Engineer, Applied Technology. Member AIAA.
†Staff Engineer, Applied Technology.
‡Senior Engineer, Applied Technology.

Introduction

HIGH-PERFORMANCE arc heaters used for re-entry vehicle materials testing are designed to operate at high pressures, mass flows, and currents, and are generally configured as long, slender pressure vessels within which electric discharges are established over lengths of several meters (Fig. 1). These long discharges are usually stabilized by the introduction of gas swirl to center the arc column on the central axis. The flow and electrical behavior in the main part of these heaters may be calculated by either the ARCFLO code,[1] or its successor code, SWIRLARC.[2] Both of these codes are simplified parabolized Navier–Stokes codes. An arc heater code that uses a three-dimensional, locally implicit, time-dependent Navier–Stokes flow solver, and includes the electromagnetic equations and a multidimensional, differential radiation model, is under development.[3] None of these codes, however, address

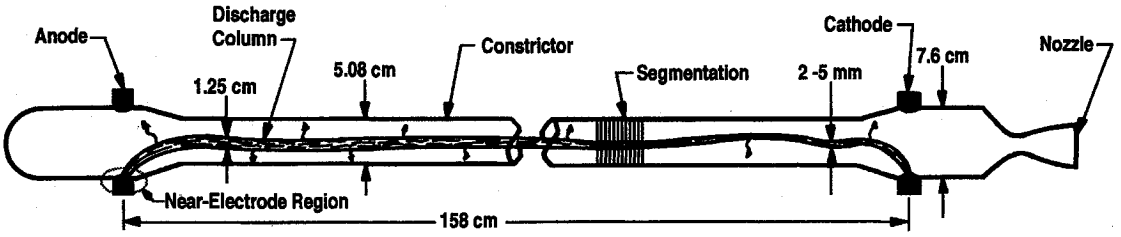

Fig. 1 Configuration of typical high-pressure, high-power arc heater.

the detailed physics of the discharge in the immediate region around the attachment to the electrode surfaces, where there is a sharp transition from gaseous to solid-state conduction of electrical current and a large increase in current density because of the large increase in electrical conductivity at the solid wall.

The gas swirl introduced for arc stability also rotates the arc attachment spots around the electrode surfaces at a rapid rate. The local energy input to the electrode surface at the moving attachment spot is a result of dissipation of electrical energy in a thin layer of gas over the attachment point, which is characterized by steep gradients of temperature, gas species concentration, and electrical potential. This thin layer has been analyzed in several papers.[4-8] Two subzones have been identified: 1) an ionization zone of typical thickness 10^{-2} cm and 2) a space-charge zone of typical thickness 10^{-4} cm. These typical dimensions indicate a spot layer so thin that it is geometrically insignificant relative to the rest of the arc heater flow. A number of authors[4-8] have treated the near-electrode region. Most of these treatments model a zone next to the wall as a space charge zone (or sheath), a noncontinuum region of a few mean free paths in thickness. The number of collisions in this zone is negligible; therefore, there is no ionization or recombination within this zone. The voltage drop in this zone is determined from a solution of the Poisson equation. It is assumed this voltage drop energy loss is totally absorbed by the wall, heating the surface and facilitating arc attachment. Outside the sheath zone is another zone, often called the ionization zone, where electron nonequilibrium effects may be present. These zones are adjacent to the wall and much thinner than the gasdynamic boundary layer; therefore, the gas velocity is negligible and the physical processes are usually formulated in a one-dimensional approximation.

Hsu and Pfender[4] analyzed the sheath zone for a cathode in an argon atmosphere at 1-atm pressure. In the ionization zone, they allow for electron thermal nonequilibrium and nonequilibrium ionization, thus requiring solution of a heavy gas energy equation, an electron energy equation, and a species equation. These results were then matched to the space charge zone where the Poisson equation was solved for the voltage drop. A slightly different approach was employed by Meeks and Capelli[5,6] using a global recombination rate parameter as one of the wall boundary conditions. This analysis was also for an electrode in argon at 1-atm pressure. Durgapal[7] used a sheath analysis plus energy balance considerations to relate wall current density, spot size, and wall temperature. Goodfellow and Polk[8] present an overall near-cathode model by combining models of the presheath/ionization, sheath, and surface regions with a cathode thermal model.

There are two aspects of the physics of the near-electrode region that are of great practical concern. First, the voltage drop across the layer, which is ultimately responsible for a greatly magnified heat flux to the electrode surface at the arc spot. This heat flux is 10^3 to 10^4 times greater than the average convective and radiative heat flux outside the arc spot. Second, an elevated surface temperature at the arc spot, which is high enough to melt the surface locally and generate mass boil-off of electrode material as a vapor.

In Refs. 9 and 10, the near-electrode region was analyzed at substantially higher pressures (100 atm) than in prior work and also matched to a three-dimensional solid (or liquid) heat conduction zone beneath the electrode surface. A redefinition of the characteristics of the near-electrode region was proposed in which the space-charge zone was replaced by a current concentration zone in which continuum joule heating was extended all the way to the wall. In this zone the entire accommodation of the large difference in electrical conductivity between gaseous and solid state was made. In Ref. 9, equilibrium ionization was assumed because of the high pressure, which permitted a solution based only upon a heavy-particle energy equation. Partial agreement with experimental observation was obtained for the cathode. In Ref. 10, nonequilibrium ionization was incorporated. Electrons in an electric field are accelerated between collisions, and this addition of energy, when thermalized by collisions, results in a Maxwellian distribution of velocities for electrons having a characteristic temperature T_e greater than the heavy particle temperature. The electron temperature determines the electron composition in a gas mixture and the electrical conductivity of the gas. Reasonable operating lines could then be predicted[10] for both the anode and cathode, but one experimental observation was still required to fix the operating point.

The present study is a refinement of the method presented in Refs. 9 and 10. Four zones are identified: 1) the flow affected zone, 2) current concentration zone, 3) surface zone, and 4) copper electrode. The zone solutions are matched utilizing a surface energy balance. The effects of field emission are accounted for in the cathode boundary condition. Theoretical criteria are developed to predict an operating point and not just an operating line. The predicted operating points are then tested against the observed attachment spot size and mass loss rates.

Approach

The concept of a space-charge sheath used by other authors[4-8] (which is a zero or low-current model) is replaced with a thicker continuum region that will be referred to as a current concentration zone. It has long been observed that, under certain conditions, electrical current concentrates in the near-electrode region; the current density in the outer flow is much lower than at the spot where it enters the electrode. This phenomenon occurs in arc heaters, magnetohydrodynamic (MHD) machines, rail guns, etc. In the approach adopted here, this experimentally observed variation in current density is imposed on the joule heating term in the heavy gas energy equation. This results in a drastically increasing heat flux as the wall is approached. Nonequilibrium ionization was assumed for both the anode and the cathode; however, use of an electron emission boundary condition for the cathode caused the cathode solution to be much closer to the equilibrium result than was the anode. The gas-phase analysis is linked to the unsteady three-dimensional solid (or liquid) heat conduction zone beneath the electrode surface for a rapidly moving arc spot.

Thermal Analysis

The near-electrode region adjacent to a wall is a very thin region compared to the flow region, hence, the flow velocities in this region are considered negligible. The solution to the conservation equations thus reduces to a heat conduction prob-

lem. The combined region is divided into four subregions or zones as shown in Fig. 2a, where the z coordinate is normal to the electrode surface. The zones to be considered are listed next, starting from the flow side. The details of the solutions in each of these zones are then discussed along with results of an example calculation.

1) The flow-affected zone consists of the entire internal flow cavity of the arc heater. The near-electrode region will be shown to be so small that it does not detract from the geometric size of the flow-affected zone. The pressure, temperature, total current, current density, and heat flux in this zone provide the outer boundary conditions for the current concentration zone. For the case analyzed here, P = 100 atm, T = 10,000–14,000 K, I = 1000 A, $J = 10^4$ A/cm^2, and heat flux toward the wall is zero. These values of I and J imply an arc column diameter of 0.36 cm in this zone.

2) In the current concentration zone, one-dimensional approximations are used and the current density undergoes transition from the flow-affected zone value to the wall value, according to an assumed variation. This approach is analogous to the classical integral boundary-layer solution where a profile shape is assumed and then subjected to the appropriate conservation equation and boundary conditions. The temperature and current density, T_w and J_w, are specified as boundary conditions at the wall side. At the other edge of the zone, the value and slope of the temperature are matched to the flow-affected zone solution, resulting in the determination of the thickness of this zone. Calculated results at this stage are values of wall heat flux (and spot size) as a function of assumed values of wall temperature and wall current density q_w, $d_s = f(T_w, J_w)$.

3) The surface zone is characterized by the electrode material work function. Electrons absorb energy at the cathode as they leave the surface while, at the anode, energy is released as electrons recombine with the surface.

4) In the copper electrode, a three-dimensional solid-state heat conduction problem is solved for an attachment spot that is moving rapidly along the surface because of rotation of the arc. This solution depends on the wall temperature, heat flux, and the spot size (or current density). Therefore, there is again a solution of the form, $q_w = f(T_w, J_w)$ for a specific U. This solution must be matched to the concentration zone solution, plus or minus the effective work function energy and latent heat.

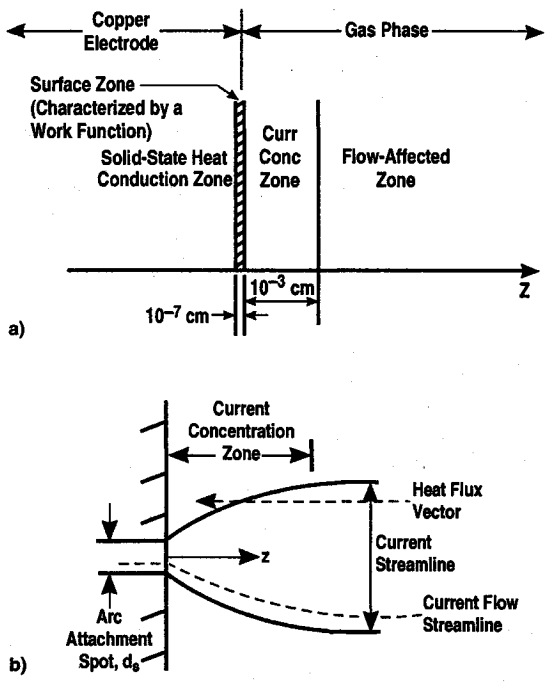

Fig. 2 Zones of near-electrode region: a) four zones considered and b) current streamtube in concentration zone.

Flow-Affected Zone

This zone will require a three-dimensional, Navier–Stokes solution for complex geometries. A complete solution of this type is not yet available. Boundary conditions for the example shown here were taken from a typical SWIRLARC[2] solution at 100 atm and consists of a current of 1000 A, a current density of 10^4 A/cm^2, a temperature of 14,000 K, and a zero heat flux. These values become boundary conditions for the near-electrode solution (specifically for the current concentration zone). A sensitivity analysis to these parameters is presented in Ref. 10.

Current Concentration Zone

J is not constant in this region, but varies from the value in the flow region to some considerably larger value at the wall, consistent with the observed small widths of arc tracks on electrode surfaces, approximately 0.4–0.6 mm. A varying-area current filament is assumed, as shown in Fig. 2b, which satisfies current density boundary conditions at either edge of the concentration zone. From a heat conduction point of view, it is noted that for gas temperatures less than 10,000 K, the thermal conductivity is dominated by the heavy particles. Therefore, the one-dimensional approximation of the heat conduction is retained, even though the current continuity is treated in a quasi-one-dimensional manner. Radiation is an important component of the solution at high pressure in the flow-affected zone. It can be neglected in the concentration zone only because it contributes a very small percentage of the wall heat flux at the arc attachment spot. With this scenario, the local value of J is determined from the quasi-one-dimensional relation: $I = J$ A. Since the total current remains constant, the heavy gas energy equation may be written as:

$$\frac{\mathrm{d}^2T}{\mathrm{d}z^2} + \frac{I^2}{\mathrm{A}^2 k\sigma} = 0 \tag{1}$$

To solve this differential equation it is necessary to determine how J varies with z. In the absence of a proper model for this dependence, an assumption will be made to obtain a solution. The character of this assumption has a marked effect on the L_c [e.g., Eq. (7)]. However, there is a compensating effect, so that the q_w is not greatly changed [e.g., Eq. (6)]. Since q_w is the important result for matching to the other zone solutions, we proceed to assume that $\sqrt{k\sigma}/J$ varies linearly with z, which also incorporates the property variation. The total variation of this parameter across the concentration layer is expressed by CR:

$$CR = (J_w/J_f)\sqrt{(k_f \sigma_f / k_w \sigma_w)} - 1 \tag{2}$$

The differential equation can be integrated by separating the variables and applying appropriate boundary conditions. The solution is

$$\frac{T - T_w}{T_f - T_w} = \frac{z}{L_c} + \frac{J_w^2 L_c^2}{(T_f - T_w) k_w \sigma_w (CR)^2} \times \left[\ell n \left(1 + \frac{z}{L_c} CR \right) - \frac{z}{L_c} \ell n(1 + CR) \right] \tag{3}$$

Differentiating and evaluating at $z = 0$ yields an expression for the heat flux at the wall:

$$q_w = k_w \left(\frac{T_f - T_w}{L_c} \right) + \frac{J_w^2 L_c}{\sigma_w CR} \left[1 - \frac{\ell n(1 + CR)}{CR} \right] \tag{4}$$

By matching the value and derivative of the temperature with the flow region solution, one obtains a quadratic equation for L_c:

$$\frac{J_w^2}{\sigma_w CRk_w}\left[\frac{1}{1+CR}-\frac{\ell n(1+CR)}{CR}\right]L_c^2 - \left(\frac{dT}{dz}\right)_{z=L_c} L_c + (T_f - T_w) = 0 \quad (5)$$

For most arc attachment applications the following further approximations can be made: 1) the axial heat flux inside the arc is small in the flow region, hence, $dT/dz = 0$ is assumed at the boundary between the flow region and the concentration region, 2) $CR \gg 1$, and 3) the temperature gradient term in Eq. (4) can be neglected compared to the joule heating term. With these simplifying assumptions, Eqs. (4) and (5) reduce to

$$q_w = J_w\sqrt{\frac{(T_f - T_w)k_w}{\sigma_w(\ell n\, CR - 1)}} = f_1(J_w, T_w) \quad (6)$$

$$L_c = \frac{CR}{J_w}\sqrt{\frac{(T_f - T_w)\sigma_w k_w}{\ell n\, CR - 1}} = f(J_w, T_w) \quad (7)$$

q_w and L_c are given independently as functions of J_w and T_w by these two simplified relations.

The ionization model assumed for the current concentration region determines the evaluation of σ_w. A general nonequilibrium is assumed wherein the electron temperature exceeds the heavy-particle temperature by an amount that depends on the electric field strength and gas pressure, expressed by the following electron energy equation[11]:

$$\frac{d}{dz}\left(k_c\frac{dT_c}{dz}\right) + \sigma E^2 - \sigma P^2\left(\frac{24\delta_h}{\pi}\right)\left(\frac{m_e}{m_h}\right)\left(\frac{Q_{eh}}{e}\right)^2 \times \left(\frac{T_e}{T}\right)\left(\frac{T_e}{T}-1\right) = 0 \quad (8)$$

The symbols are as defined in the Nomenclature. At the anode wall the boundary condition is expressed as a balance between the last two terms in Eq. (8), i.e., the second derivative term is assumed negligible. (Incidentally, the last two terms are dominant inside the region as well.) The electron temperature distribution obtained for this general nonequilibrium assumption is shown as the anode solution in Fig. 3. In the case of the cathode, it is necessary to use as a wall boundary condition the electric field required for field emission of the assumed J_w from a copper surface at T_w (see Fig. 4). This results in an electron temperature distribution much closer to the equilibrium case (see Fig. 3). In each case, σ_w is determined by T_{ew}.

Copper Heat Conduction Zone

The surface heat flux/temperature combinations resulting from the gas-phase calculations must be matched to corresponding values for three-dimensional heat conduction into solid copper for an arc spot moving rapidly over the surface. For an observed rotation rate of 250 Hz inside a 7.6-cm-diam electrode ring, the linear speed of the moving arc spot is U = 60 m/s. The heat pulse in the copper is unsteady in a reference frame fixed to the electrode, but it produces a steady temperature profile in a reference frame that moves with the arc spot. The temperature rise over the arc spot is superimposed on a steady average temperature of 800 K for the rest of the electrode, determined from measured average cooling losses and the known electrode wall thickness. The use of a steady background temperature is valid because of the following:

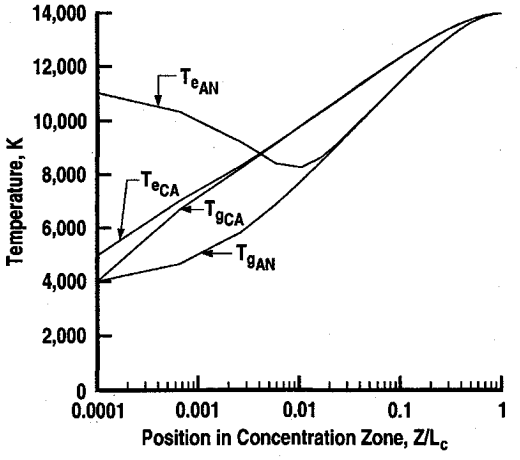

Fig. 3 Typical electron and heavy gas temperature distributions in current concentration zone, for T_w = 4000 K, $J_w = 10^6$ A/cm^2, $J_f = 10^4$ A/cm^2, I = 1000 A, T_f = 14,000 K, P = 100 atm, and q_f = 0.

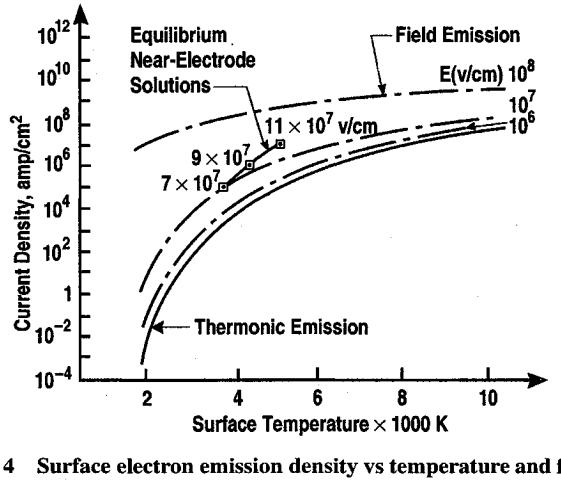

Fig. 4 Surface electron emission density vs temperature and field strength.

1) An examination of a used electrode shows the arc tracks criss-crossing the electrode surface rather than returning to the same spot on each revolution.

2) The path length for one revolution is some 500 spot diameters, giving ample time for the backside water cooling to dissipate the residual energy.

To facilitate analysis, an available analytical solution for three-dimensional heat conduction into a solid from a square heat source of q_w moving along the surface of a semi-infinite medium at a velocity U in the x direction was used.[9,12] The heat source covered the span $-b < x < b$ and $-b < y < b$ on a surface $z = 0$. The temperature increase is

$$\Delta T(x, y, z) = \frac{1}{2\sqrt{2\pi}}\left(\frac{Kq_w}{kU}\right)\int_0^\infty \exp\left(\frac{-z^2}{2u}\right) F_1(Y)F_2(X)\frac{du}{\sqrt{u}} \quad (9)$$

where

$$F_1 = \text{erf}[(Y + B)/\sqrt{2u}] - \text{erf}[(Y - B)/\sqrt{2u}]$$

$$F_2 = \text{erf}[(X + B + u)/\sqrt{2u}] - \text{erf}[(X - B + u)/\sqrt{2u}]$$

Solutions for the dimensionless temperature rise over the surface are readily obtained as parametric functions $B = Ub/2K$, which involves the velocity and the K (Fig. 5). The maximum temperature rise on the surface occurs near the trailing edge of the profile ($x = -b$, $y = 0$). For linking to the gas-

phase calculations, however, the average surface temperature of the arc spot was used, given by ΔT_{av}, obtained by integration over the entire heat pulse, and found to be $\Delta T_{av} = 0.608\Delta T_{max}$ for $B > 10$. As will be seen, the surface heat fluxes resulting from the gas phase calculations are high enough to heat the copper well above its melting temperature of 1357 K, even as the arc spot translates rapidly across the surface. A moving zone of molten copper results, with a length directly related to q_w and inversely related to the traverse speed U. Typical melt-zone contours are given in Fig. 6 for a 10-MW/cm^2 heat source moving at U = 60 m/s over an 800 K copper surface. The isotherms were obtained for copper conductivity and diffusivity of k = 3.87 W/cm K, K = 1.13 cm^2/s, B = 13.3, and with the solution modified to circular geometry by an approximate correction based on the correspondence between moving and fixed heat-source solutions in which time of exposure to the fixed heat source is linearly related to position within the moving heat source. The correspondence is valid only for large values of B (high velocity and/or low thermal diffusivity), such that transverse and longitudinal flow of heat are small and the heat conduction is predominantly one dimensional into the solid medium.

Solution Matching

The gas-phase solution must be matched to the solid electrode solution, taking into account the work function. The surface work function for copper is 4.65 eV. The wall heat flux will then be augmented by ϕJ_w at an anode, and diminished by $\phi_{eff} J_w$ at a cathode (ϕ_{eff} is discussed in the next paragraph). For a given total current of 1000 A and a gas static pressure of 100 atm, and using CR as a parameter, values of q_w and T_w were determined that simultaneously satisfy both the gas-phase

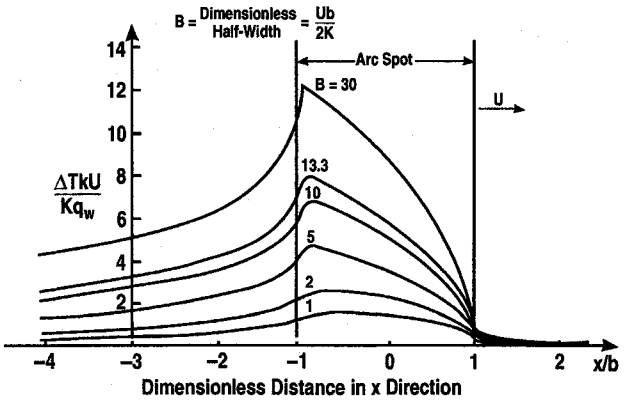

Fig. 5 Dimensionless temperature rise for square heat pulse moving in X direction, $y/b = z/b = 0$.

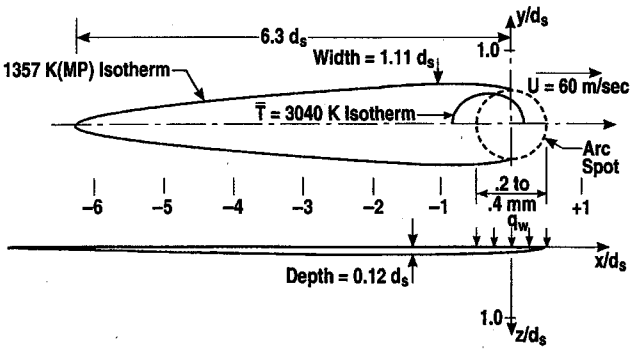

Fig. 6 Molten copper zone produced by moving arc spot, q_w = 10 MW/cm^2 and B = 13.3.

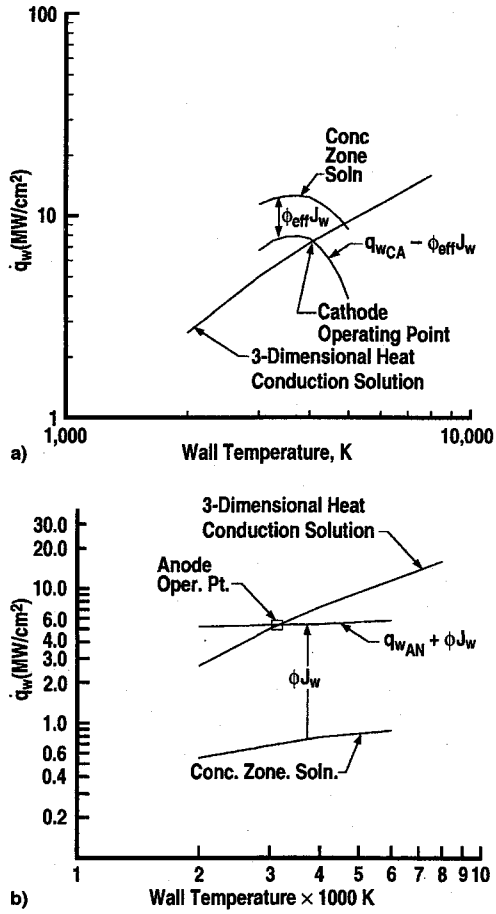

Fig. 7 Simultaneous solution of concentration and heat conduction zones, for $J_w = 10^6$ A/cm^2, d_s = 0.36 mm, and T_f = 14,000 K: a) cathode and b) anode.

calculations and the three-dimensional solid-state heat conduction calculations in the copper. The solutions (q_w vs T_w for one value of wall current density, $J_w = 10^6$ A/cm^2) are shown in Fig. 7 for the concentration region (cathode and anode) and also for the copper heat conduction region. Additional lines are shown for the gas-phase side: 1) the concentration solution minus the effective work function for the cathode and 2) the concentration region plus the work function for the anode. The intersection of these curves with the copper heat conduction solution yields cathode and anode operating points for this specific current density at the wall. Since the total current for this example is 1000 A, a current density of 10^6 A/cm^2 implies a spot size of 0.357 mm diameter. Repeating this process for other current densities (i.e., spot sizes) allows the definition of possible cathode and anode operating lines.

Cathode

At high surface temperatures, thermionic emission is the dominant current conduction mechanism at a cathode surface. Thermionic emission is described by the empirical Richardson–Dushman relation shown in Eq. (10). Especially significant at lower surface temperatures, emission may be enhanced by a surface electric field, a phenomena known as the Schottky effect.[8,13] This effect can be expressed as a reduction of the material work function in Eq. (11).

$$J = A_R T_w^2 \exp(-\phi_{eff}/k_B T_w) \tag{10}$$

$$\phi_{eff} = \phi_0 - [eE_w/(4\pi\varepsilon_0)]^{0.5} \tag{11}$$

In the parametric calculations done here, the electric field required to supply the assumed current density is computed from

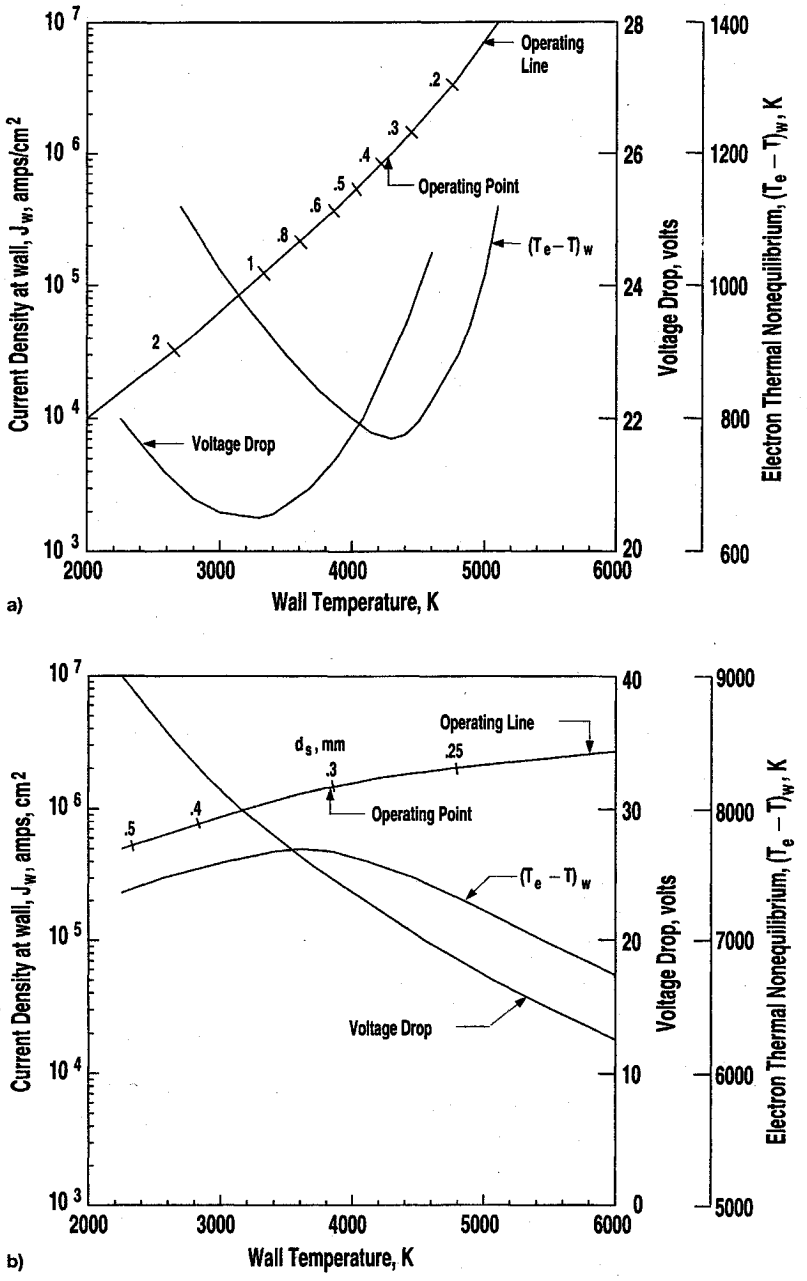

Fig. 8 Electrode operating lines, P = 100 atm, T_f = 14,000 K, and $J_f = 10^4$ A/cm^2: a) cathode and b) anode.

Eqs. (10) and (11). The electrical conductivity at the wall is computed from Ohm's law and the value of electron temperature required to produce this conductivity is computed. This resulting value of T_{ew} was used as the wall boundary condition for the electron energy equation, Eq. (8). It is noted that for the cathode, the heat transfer from the concentration zone must be large enough to supply the effective work function energy plus drive the solid body heat conduction process. The intersection of the $(q_{\text{cathode}} - \phi_{\text{eff}} J_w)$ line with the solid body (electrode) heat conduction line (Fig. 7a) thus represents the cathode operating point at the specified parametric value of current density (10^6 A/cm^2). The results presented in Fig. 7 are for one wall current density. As noted before, repeating this process for other current densities (i.e., spot sizes) allows definition of possible cathode and anode operating lines as depicted in Fig. 8.

In addition to the operating line, curves for the difference between the electron and heavy gas temperatures $(T_e - T)_w$, at the electrode surface and the total voltage drop across the concentration layer, are shown in Fig. 8. In the case of the cathode (Fig. 8a), both of these curves exhibit minima. Since the total current is constant across the concentration layer, the minimum voltage point is also a minimum power point. Minimum energy considerations would lead to a predicted operating point of about 3400 K. However, since field emission is significant and electrons are being extracted with as low an energy as possible, it is felt that the dominant tendency would be to operate at the point of minimum electron thermal nonequilibrium. Therefore, the predicted operating point for the cathode is at T_w = 4259 K.

Anode

At the anode the electrons will be entering the electrode and releasing the work function energy. Here, a nonequilibrium boundary condition is used at the wall with the degree of nonequilibrium determined by Eq. (8). It is noted from Fig. 7b that with this assumption the heat transfer from the concentration region is small compared to the work function energy. In other words, at the anode, nearly all of the energy to drive the solid body heat conduction process is supplied by the work

function. Hence, the anode and cathode mechanisms are fundamentally different, in spite of the fact that the operating points are relatively close together in terms of electrode wall temperature, heat load on the electrode, and spot size.

This different behavior at the anode is also evident in Fig. 8b. The voltage drop is seen to decrease monotonically with increasing temperature; therefore, minimum energy considerations would shift the operating point in the direction of ever-increasing electrode surface temperature. $(T_e - T)_w$ exhibits a maximum at 3783 K. In contrast to the cathode where electrons are being extracted at relatively low energy by the field emission mechanism, at the anode, the electrons have been accelerated through the entire voltage drop between cathode and anode and are at a relatively high-energy level. The electrons will relinquish their work function energy as they enter the anode surface. This abundance of energy released near the surface will give rise to a considerable amount of electron thermal nonequilibrium in that region, as can be seen in Fig. 3. Therefore, the maximum $(T_e - T)_w$ occurring at $T_w = 3783$ K (see Fig. 8b) is the most probable operating point for the anode.

Comparison with Experimental Data

The extremely high pressures and temperatures inside a high-performance arc heater are not conducive to detailed and direct diagnostic measurements at the arc spot. Most information obtained on arc spot characteristics is of an indirect nature. Rate of translation of the arc attachment over the electrode surface is obtained from high-speed motion pictures of the rotating arc taken through quartz windows in the heater walls. Dimensions of arc spot tracks on recovered electrode rings have been measured. Also, careful monitoring of the weight of electrode rings over a large number of runs provides a means to assess the rate of mass loss from the rotating, molten arc spots.[9,10] Such information is compared with predicted characteristics of the arc spot operating points (Fig. 8a for the cathode and Fig. 8b for the anode) in Table 1.

Width of Arc Tracks

At the extremes of arc foot motion, beyond the area where there have been thousands of crossings and recrossings, a limited number of individual tracks of the arc spot are observable on recovered electrode rings. After careful removal of oxide slags, these tracks have been found to be shallow grooves in the copper, with widths of 0.38–0.64 mm, much smaller than the apparent diameter of the arc column away from the electrode (5–8 mm). It may be seen in Table 1 that the attachment spot diameters predicted by the current concentration model (0.38 mm for cathode and 0.30 mm for anode) are in reasonable agreement with the measureable arc track widths. Referring to Fig. 8a, a projected cathode operating point at the minimum voltage drop across the concentration layer implies an arc spot diameter greater than 1 mm, substantially larger than the observed track widths. This supports the conclusion that the cathode operating point tends toward minimum electron thermal nonequilibrium rather than minimum voltage drop.

Mass Loss from Electrodes

Release of copper electrode material from a rapidly moving molten arc spot can result from one or more different mechanisms: 1) simple surface evaporation from the molten region of the arc spot that lies within the circle of electric current, 2) an increased mass loss by subsurface nucleate boiling, 3) scrubbing of molten material by viscous forces, or 4) bodily ejection of molten droplets by a large excess of copper vapor pressure above the background hydrostatic pressure. Given the current analysis capability, it is not possible to specify the exact combination of these mechanisms that are active in any given case, but it does appear possible to define both the minimum and maximum rates of mass removal that are possible.

Minimum Loss Rate

All areas of the moving arc spot, where the surface temperature is greater than the 1357 K melting temperature, will be releasing copper vapor by surface evaporation at the classical rate, defined by kinetic theory and the equilibrium vapor pressure relation[14,15]:

$$(\dot{m}/A)_{\text{evap}} = 10^{(5.6397 - 16204/T_w)} \left[m_{\text{Cu}}/(2\pi k T_w)^{0.5}\right] \tag{12}$$

Outside the current column, the net mass flow from the molten surface is much lower than this because of the diffusion limitation at high hydrostatic pressure. Inside the current column, however, there is a strong macroscopic pumping of mass flow away from the surface, produced by the macroscopic gradient of the magnetic pressure within the arc column:

$$p_M = B_i^2/(2\mu_0) = \mu_0 I^2/(8\pi^2 r_A^2) \tag{13}$$

This pressure increases rapidly near the surface, where r_A becomes very small in the concentration zone. The mass acceleration produced by this gradient in pressure, for the spot size and contraction ratio of the present study, is capable of producing a mass flow of 3×10^{-3} to 4.5×10^{-3} kg/s in a macroscopic jet away from the surface. The copper vapor released at the surface is only 6–10% of this flow and is entrained with it at a rate that is orders of magnitude higher than the diffusion-limited rate.

An approximate solution of the axially symmetric momentum and continuity equations results in the flow behavior shown qualitatively in Fig. 9. Only the direction, not the magnitude, of the velocity vectors is indicated. Integration of the evaporation release of Eq. (12) over the nonuniform arc spots defined in Table 1 results in projected mass loss rates for the cathode and anode spots of 1.59×10^{-3} kg/s and 4.22×10^{-4} kg/s, respectively. When an allowance for latent heat of fusion for copper of 0.2049 MJ/kg is subtracted from the incoming heat flux, the evaporation rates are reduced to 9.8×10^{-4} kg and 2.4×10^{-4} kg/s from cathode and anode, respectively. These values are compared with mass loss rates produced by other mechanisms in Fig. 10.

Table 1 Predicted and measured cathode and anode characteristics

Operating point characteristic for $I = 1000$ A, $P = 100$ atm, and $J_f = 10^4$ A/cm^2	Cathode predicted	Anode predicted	Experiment observation (both electrodes)
Condition	$(T_e > T)_{\min}$	$(T_e - T)_{\max}$	——
Average spot temperature, K	4259	3783	——
Wall current density, A/cm^2	8.71×10^5	1.4×10^6	——
d_s, mm	0.38	0.30	0.38–0.64
Wall heat flux, MW/cm^2	7.54	7.28	——
Heat flux from concentration zone, MW/cm^2	11.4	0.6	——
Concentration ratio	87	140	——
B	50.7	40.2	——
Voltage drop, V	23	25	——
Maximum temperature (with latent heat), K	6125	5342	——
Integrated evaporation rate, kg/s	9.8×10^{-4}	2.4×10^{-4}	2.6×10^{-4}

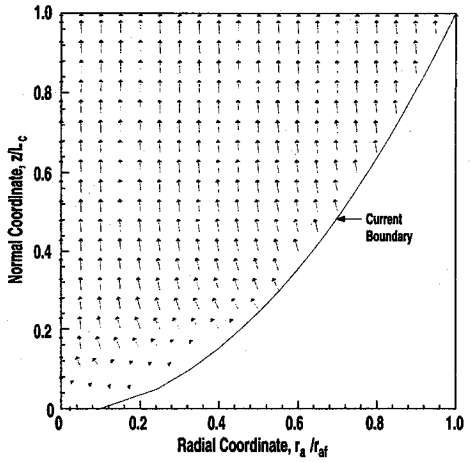

Fig. 9 Velocity field in the concentration zone caused by the gradient in the magnetic pinch pressure.

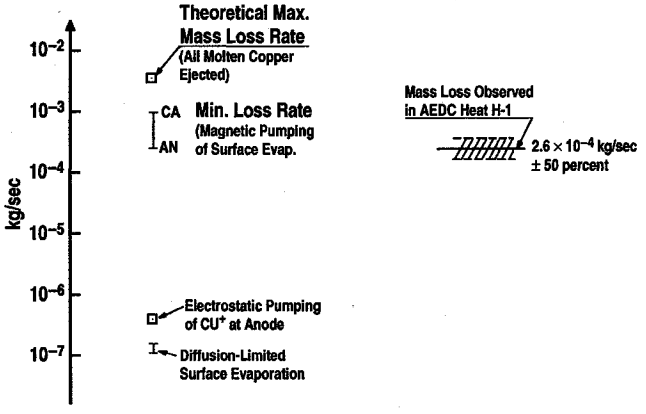

Fig. 10 Electrode mass loss rates, I = 1000 A and P = 100 atm.

Maximum Loss Rate

When electromagnetic pumping of surface evaporation is supplemented with mass loss by more stringent processes, it appears a maximum rate could be represented by assuming a bodily removal of all the copper that is melted at any location over which the arc spot passes. The three-dimensional moving-spot heat conduction solutions, previously described, indicate a maximum melt-zone cross section occurring approximately three spot diameters past the spot trailing edge, where it is a little over a diameter wide and approximately 5% of the diameter deep. For the larger (cathode) spot, the cross section of the melt-zone is 6.8×10^{-3} mm^2. This cross section moving at the spot velocity of 60 m/s results in a maximum molten copper rate of

$$\dot{m}_{Cu} = \rho AV = (8950 \text{ kg/m}^3)(6.8 \times 10^{-9} \text{ m}^2)(60 \text{ m/s})$$

$$= 3.65 \times 10^{-3} \text{ kg/s}$$

If all of this copper left the surface of the electrode ring without major redistribution of the three-dimensional temperature profiles, it should represent the potential maximum removal rate, also indicated in Fig. 10.

The copper loss rate observed in the H1 arc heater (2.6×10^{-4} kg/s), averaged over many runs at 100-atm pressure and 1000-A current, is much closer to the minimum mass loss rate corresponding to electromagnetic pumping of the surface evaporation from the arc spot than it is to the maximum loss rate postulated for bodily removal of the entire amount of melted copper. It is encouraging that there is at least an order of magnitude agreement between observed and computed mass loss rates, considering the approximations in both the concentration zone solution and in the conduction zone calculations. There is disagreement, however, in the fact that calculated cathode and anode rates differ by a factor of 4, whereas the observed rates are nearly indistinguishable (see Table 1). This may be an indication that the actual mass loss may not be so much because of evaporation as to bodily ejection of molten copper from the moving arc spot.

Summary

A continuum model has been formulated for the near-electrode region in a high-pressure arc heater in which the arc attachment point moves at high velocity over an electrode surface. The model extends from the flow region all the way into a copper electrode, and thereby accommodates the large change in electrical conductivity that occurs at the gas/solid interface of the electrode. The gas phase portion of the model is a simple current concentration zone in which the gas energy equation is satisfied in a one-dimensional approximation. It was found necessary to incorporate a field-emission boundary condition at the cathode spot and a nonequilibrium electron temperature at the anode spot. Heat conduction into the solid copper electrode is modeled in three dimensions in a reference frame, which moves with the arc spot and in which the thermal solution is steady state. A family of joint solutions of the gas-phase energy equations and the three-dimensional heat conduction problem in the solid was developed by doing a surface energy balance that accounted for the work function energy. Operating points were fixed on the anode and cathode operating lines by determining points of maximum and minimum electron thermal nonequilibrium, respectively.

Predicted values of arc spot size and electrode mass loss were compared with observations. The values predicted for arc spot size were in good agreement with observed values for both anode and cathode. Mass loss values are in excellent agreement with predictions for the anode. The predicted mass loss for the cathode is over three times larger than the observed value. For a high-pressure arc heater, the measured mass loss for the cathode is found to be the same as for the anode, within experimental error. This discrepancy may be because of the uncertainty involved in selecting the dominant mass loss model.

Acknowledgments

This research was performed by the Arnold Engineering Development Center (AEDC), Air Force Materiel Command. Work and analysis was performed by personnel of Sverdrup Technology, Inc., AEDC Group, Technical Services Contractor.

References

[1]Nicolet, W. B., Shepard, C. E., Clark, K. J., Balakrishnan, A., Kesselring, J. P., Suchsland, K. E., and Reese, J. J., Jr., "Analytical and Design Study for a High-Pressure, High-Enthalpy Constricted Arc Heater," Arnold Engineering Development Center, TR-75-47 (AD-A012551), Arnold AFB, TN, July 1975.

[2]Shaeffer, S. F., "SWIRLARC: A Model for Swirling, Turbulent, Radiative Arc Heater Flowfields," AIAA Paper 78-68, Jan. 1978.

[3]Felderman, E. J., Chapman, R., and Jacocks, J. L., "Development of a High-Pressure, High Power Arc Heater: Modeling Requirements and Status," AIAA Paper 94-2658, June 1994.

[4]Hsu, K. C., and Pfender, E., "Analysis of the Cathode Region of a Free-Burning High Intensity Argon Arc," *Journal of Applied Physics*, Vol. 54, July 1983, pp. 3818–3824.

[5]Meeks, E., and Cappelli, M. A., "A Multi-Fluid Model of Near-Electrode Plasma Behavior," AIAA Paper 93-2103, July 1993.

[6]Meeks, E., and Cappelli, M. A., "Two-Temperature Model for High-Pressure Plasmas in Contact with Cooled Electrodes," *Journal of Applied Physics*, Vol. 73, April 1993, pp. 3172–3182.

[7]Durgapal, P., "Electrode Phenomena in High-Current, High-Pressure Arc Heaters," *Journal of Thermophysics and Heat Transfer*, Vol. 7, No. 3, 1993, pp. 412–417.

[8]Goodfellow, K. D., and Polk, J. E., "High Current Cathode Thermal Behavior, Part I: Theory," International Electric Propulsion Conf., Paper 93-030, Sept. 1993.

[9]Felderman, E. J., MacDermott, W. N., and Fisher, C. J., "Near-Electrode Model at High Pressure (100 atm)," AIAA Paper 94-2039, June 1994.

[10]Felderman, E. J., and MacDermott, W. N., "Near-Electrode Model with Nonequilibrium Ionization (at 100 atm)," AIAA Paper 95-1993, June 1995.

[11]Sutton, G. W., and Sherman, A., *Engineering Magnetohydrodynamics*, McGraw–Hill, New York, 1965, p. 148.

[12]Carslaw, H. S., and Jaeger, J. C., *Conduction of Heat in Solids*, Oxford Univ. Press, Oxford, England, UK, 1959, p. 270.

[13]Cobine, J. D., *Gaseous Conductors*, Dover, New York, 1958, p. 118.

[14]*CRC Handbook of Chemistry and Physics*, 61st Ed., CRC Press, Boca Raton, FL, 1980, p. D-221.

[15]Kennard, E. H., *Kinetic Theory of Gases*, McGraw–Hill, New York, 1938.